Observational Evidence for a Stability Iris Effect in the Tropics

Marion Saint-lu, Sandrine Bony, Jean-Louis Dufresne

Geophysical Research Letters

RESEARCH LETTER
10.1029/2020GL089059

Observational Evidence for a Stability Iris Effect in the Tropics

Marion Saint-Lu[1], Sandrine Bony[1], and Jean-Louis Dufresne[1]

[1]Laboratoire de Météorologie Dynamique (LMD)/Institut Pierre Simon Laplace (IPSL), Sorbonne Université/CNRS/École Normale Supérieure/École Polytechnique, Paris, France

Key Points:
- Space-borne lidar observations show that anvil clouds rise and reduce their coverage when the tropics warm
- Observations and meteorological reanalyses support the stability Iris effect mechanism
- There is evidence for a stability Iris effect over a large range of spatial scales

Correspondence to:
M. Saint-Lu,
marion.saint-lu@lmd.jussieu.fr

Citation:
Saint-Lu, M., Bony, S., & Dufresne, J.-L. (2020). Observational evidence for a stability Iris effect in the tropics. *Geophysical Research Letters*, *47*, e2020GL089059. https://doi.org/10.1029/2020GL089059

Received 27 MAY 2020
Accepted 30 JUN 2020
Accepted article online 8 JUL 2020

Abstract Anvil clouds cover extensive areas of the tropics, and their response to global warming can affect cloud feedbacks and climate sensitivity. A growing number of models and theories suggest that when the tropical atmosphere warms, anvil clouds rise and their coverage decreases, but observational support for this behavior remains limited. Here we use 10 years of measurements from the space-borne CALIPSO lidar to analyze the vertical distribution of clouds and isolate the behavior of anvil clouds. On the interannual time scale, we find a strong evidence for anvil rise and coverage decrease in response to tropical warming. Using meteorological reanalyses, we show that this is associated with an increase in static stability and with a reduction in clear-sky radiatively driven mass convergence at the anvil height. These relationships hold over a large range of spatial scales. This is consistent with the stability Iris mechanism suggested by theory and modeling studies.

Plain Language Summary Anvil clouds cover about 40% of the tropics. Their response to global warming, especially changes in their height or in their horizontal extent, has the potential to affect the Earth's surface temperature. By analyzing 10 years of observations of the vertical distribution of clouds from a space-borne lidar, we show that the anvils rise and reduce their coverage during the years that are anomalously warm. By using meteorological reanalyses, we further show that this behavior is consistent with the stability Iris effect suggested by theory and modeling studies. These results improve our physical understanding of the response of tropical clouds to warming and present relationships that may be used to test climate models.

1. Introduction

Anvil clouds cover extensive areas of the tropics, reflect solar radiation, and reduce outgoing long-wave radiation. In case global warming would affect their height and coverage, this could influence climate sensitivity (Hartmann, 2016; Su et al., 2017; Zelinka & Hartmann, 2010). The fixed anvil temperature (FAT) hypothesis states that anvils rise nearly isothermally when the tropics warm (Hartmann & Larson, 2002). According to FAT, anvils are formed by convective detrainment, and the altitude of maximum detrainment is constrained, through mass conservation, by the convergence of mass in the surrounding clear-sky upper troposphere. The latter is due to the vertical gradient of subsidence, which is primarily driven by the decrease with height of the radiative cooling by water vapor. The variation of water vapor with height is very much constrained by the Clausius-Clapeyron thermodynamical relationship, and therefore, the temperature at which the clear-sky radiative cooling drops is relatively invariant with surface temperature. When the surface warms, it rises in step with the isotherms, and therefore, the peaks of the clear-sky radiatively driven mass convergence and of the associated convective detrainment rise. Zelinka and Hartmann (2010) refined this theory and formulated the proportionally higher anvil temperature (PHAT) hypothesis, which states that anvils do not rise strictly isothermally but slightly warm instead, due to the sharp increase of static stability with height in the upper troposphere. Several studies have provided observational support for this theory, showing the rise of high clouds during the very strong 1997–1998 El Niño event (Xu et al., 2005), the invariance of high clouds temperature relative to surface temperature over a 6-month period (Eitzen et al., 2009; Xu et al., 2007), and the good correspondence between vertical profiles of cloud fraction and radiatively driven clear-sky mass convergence over a 10-month period (Kubar et al., 2007). These observations were then confirmed on longer periods of 4 to 6 years (Li et al., 2012; Thompson et al., 2017; Zelinka & Hartmann, 2011).

Analyzing geostationary satellite data, Lindzen et al. (2001) suggested that anvils also reduce their coverage when the tropics warms. This behavior was referred to as an "Iris effect," by analogy with the eye's iris. These observational results have been rebutted, primarily on methodological grounds (Del Genio & Kovari, 2002; Hartmann & Michelsen, 2002). Nevertheless, whether or not an Iris effect operates in climate remains an open question (Bony et al., 2015; Mauritsen & Stevens, 2015). Zelinka and Hartmann (2011) observed a reduction in the tropical high clouds cover when the tropics warm, using various satellite data including CloudSat radar observations (Stephens et al., 2017), which were only available for 4 years at that time (including one El Niño event and one La Niña event). Choi et al. (2017) focused on the western tropical Pacific and observed that convective clouds "concentrate" when the sea surface temperature rises. However, observing such a limited region does not allow to conclude on inherent cloud responses to surface temperature changes, since cloud systems can shift in and out of the box, due to dynamical effects. More recently, using various satellite observations over 13 years for the longest, Su et al. (2017) and Liu et al. (2017) reported a decrease of tropical high cloud fraction in response to interannual surface warming. Su et al. (2017) proposed that it was linked to the tightening of the ascending branch of the Hadley circulation, although the mechanism underlying the cloud fraction decrease was not investigated in details.

In models, tropical warming can also be associated with a reduction of anvil coverage (Bony et al., 2016; Cronin & Wing, 2017; Khairoutdinov & Emanuel, 2013; Tompkins & Craig, 1999; Su et al., 2017; Zelinka & Hartmann, 2010). With the idea that the reduction of anvil coverage could be linked to their elevation and to PHAT, Bony et al. (2016) proposed a thermodynamic "stability Iris" hypothesis. As the tropics warm, the anvils rise and find themselves in a more stable atmosphere, due to the lower air pressure that increases static stability. The stability Iris hypothesis states that the increased stability reduces the magnitude of the radiatively driven clear-sky mass convergence at the height of anvil clouds, thus weakening convective detrainment at that height, leading to a reduction of the anvil coverage. Several climate models and convection-resolving models have provided support for this hypothesis (Bony et al., 2016; Cronin & Wing, 2017; Zelinka & Hartmann, 2010), but the existence of the stability Iris effect in nature remains an open question.

To investigate the existence of the stability Iris effect in observations, we use lidar observations derived from the A-train Cloud-Aerosol Lidar and Infrared Pathfinder Satellite Observations (CALIPSO) (Stephens et al., 2017; Winker et al., 2017), together with ERA5 meteorological reanalyses (Hersbach et al., 2019). Lidar measurements from CALIPSO provide the most accurate cloud vertical profile measurements without time drift (Winker et al., 2007, 2017) and on a very fine vertical resolution (60 m). Here we use 10 years of data that include two El Niño and three La Niña events, to examine the behavior of the anvil cloud fraction as the tropics undergo warming or cooling events. In order to test the robustness of our results, and to determine whether they could emerge at coarser vertical resolutions of climate models, we also use the General Circulation Model (GCM)-Oriented CALIPSO Cloud Product (GOCCP) (Chepfer et al., 2010). We further investigate the existence of PHAT in these observations, as well as the spatial scale at which PHAT and the stability Iris potentially hold.

2. Data and Methods

2.1. Detection of Anvils in CALIPSO Observations

In this study, we refer to anvils as the detraining top of deep convective clouds, which lie above 8 km in the tropics (Yuan et al., 2011). To identify tropical anvils, we use the monthly mean three-dimensional cloud fraction derived from the lidar level 3 cloud occurrence product (CAL_LID_L3_Cloud_Occurrence-Standard-V1-00, Winker, 2018), hereafter CALIPSO-Cloud-Occurrence. CALIPSO-Cloud-Occurrence is gridded on 2° latitude × 2.5° longitude and on the native CALIOP vertical resolution of 60 m (344 vertical levels). We use it over the tropical belt (30°N–30°S), averaged over day and night, from June 2006 to December 2016 (10 years). Results are replicated with GOCCP (Chepfer et al., 2010) at the end of section 4.1, in order to test both their robustness and the ability of GCMs to reproduce them. GOCCP provides the monthly mean cloud fraction gridded on a 2° × 2° horizontal grid with a degraded vertical resolution of 480 m (40 vertical levels), from June 2006 to December 2017 (11 years).

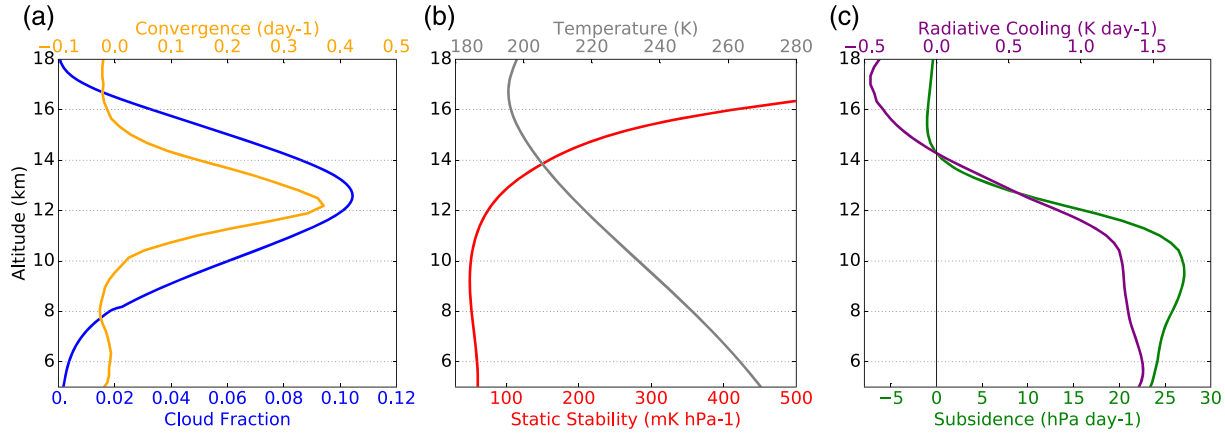

Figure 1. Vertical profiles, averaged over the tropics and over 2006–2016, of (a) cloud fraction averaged over locations with anvils only (blue) and radiatively driven clear-sky mass convergence ($\partial\omega_r/\partial p$, orange), (b) atmospheric static stability (S, red) and temperature (grey), and (c) clear-sky radiative cooling (Q_r, purple) and radiatively driven clear-sky pressure velocity (ω_r, green).

For each month and location ($2° \times 2.5°$ grid points), we define the altitude and the cloud fraction of anvil clouds, respectively Z_{anv} and CF_{anv}, where there is a local maximum of optically thick but non-opaque ice clouds coverage (optical depth $0.3 \leq \tau$%3C5), imposing that this maximum occurs above 8 km and that its cloud fraction exceeds a threshold value referred to as CF_c (we use CF_c=0.03). To disregard small maxima due to noise in the CALIPSO-Cloud-Occurrence product, local maxima are determined after having smoothed the cloud fraction profile with a 480-m running mean. If several local maxima are identified, Z_{anv} is defined by the altitude of the one closest to the cloud fraction centroid. Locations that are cloud free or where no maximum exceeds CF_c are masked and ignored. Our results do not critically depend on the details of the method used to determine Z_{anv} (not shown).

This definition of anvils excludes clear-sky regions, as well as subvisible cirrus clouds, and the cores of deep convective clouds. These choices will be tested and discussed in section 4. As will be shown, the conclusions of this study do not critically depend on the value of CF_c, nor on the exact range of optical depths considered. Figure 1a shows the annual mean cloud fraction profile averaged over locations where anvils have been detected (locations void of anvils are ignored), within the tropical belt (30°N–30°S), considering thick but non-opaque ice clouds with $CF_{anv} \geq 0.03$ (CF_c).

2.2. Clear-Sky Variables From ERA5

According to PHAT, anvils form at the altitude of the peak of upper tropospheric horizontal mass divergence in convective regions, which coincides with a peak of radiatively driven mass convergence in clear-sky regions (Hartmann & Larson, 2002; Zelinka & Hartmann, 2010). The radiatively driven clear-sky pressure velocity (ω_r, positive downward) and divergence (D_r) are diagnosed as

$$D_r = \max\left(\frac{\partial \omega_r}{\partial p}\right), \text{ with } \omega_r = \frac{Q_r}{S} \text{ and } S = \frac{TR}{pc_p} - \frac{\partial T}{\partial p} \quad (1)$$

where Q_r is the clear-sky radiative cooling rate, p the air pressure, S the static stability, T the temperature, R the gas constant, and c_p the isobaric specific heat of dry air.

We use monthly mean clear-sky radiative cooling, temperature, and pressure from ERA5 reanalyses in the tropics, horizontally regridded onto the CALIPSO-Cloud-Occurrence $2° \times 2.5°$ grid, with a vertical resolution of about 300 m in the upper troposphere (137 vertical levels in the whole atmosphere), from June 2006 to December 2017. We compute the peak of upper tropospheric horizontal mass divergence at each month and location, which is simply defined as its maximum. The altitude of this peak is referred to as Z_{Dr}.

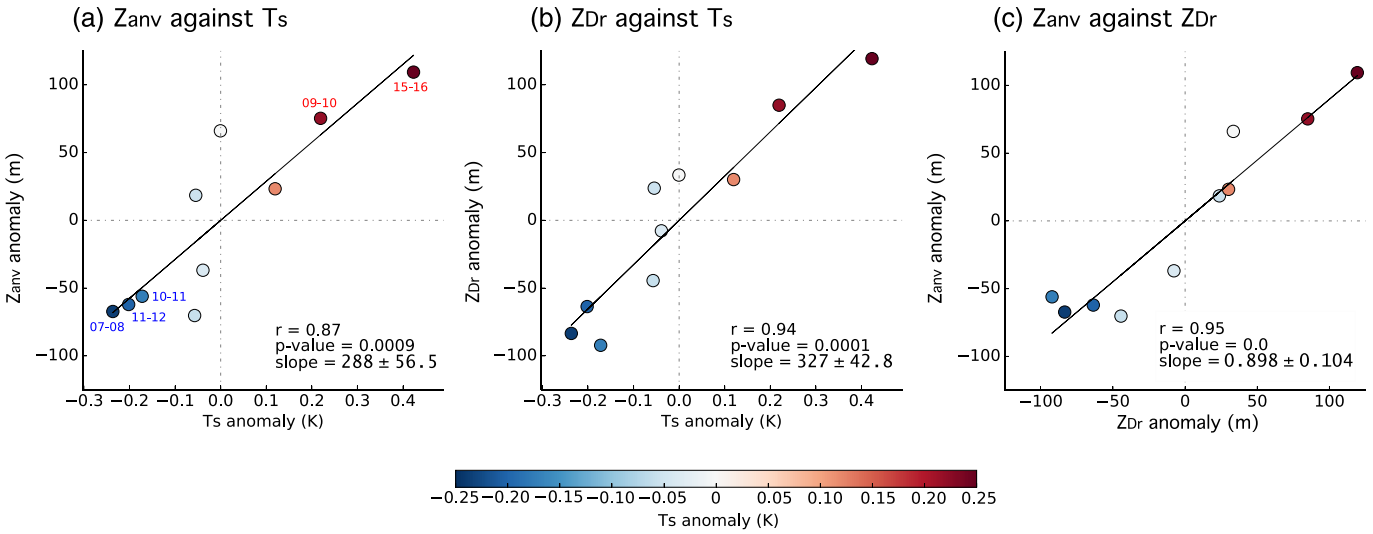

Figure 2. Scatterplots showing tropically averaged yearly anomalies (each dot is a July-to-June year, anomalous relative to the time mean over 2006–2016). Linear regressions are also reported (black lines) together with the Pearson correlation coefficient r, the p value, and the slope. Colors show the tropical mean surface temperature anomaly and numbers (a) given the corresponding year of El Niño (red) and La Niña (blue) events. The relationships involve the anvil altitude Z_{anv}, the tropical surface temperature T_S, and the divergence peak altitude Z_{D_r}.

Figures 1b and 1c show that the annual mean tropically averaged Q_r (in purple) weakens in the upper troposphere above 10 km, while S (in red) sharply increases above 12 km. As a consequence, the radiatively driven clear-sky subsidence (ω_r, in green) weakens above 10 km. Following this, Figure 1a shows that the radiatively driven clear-sky mass convergence ($\partial\omega_r/\partial p$, in orange) peaks near 12 km, at about 216 K (Figure 1b), and the anvil cloud fraction profile (in blue) peaks near 12.5 km, at about 214 K. The anvil cloud fraction profile thus exhibits a clear correspondence with the radiatively driven clear-sky mass convergence profile.

2.3. Surface Temperatures from HadCRUT4

Monthly land and sea surface temperatures (T_s) are derived from HadCRUT4 (Morice et al., 2012) in the tropics, from June 2006 to December 2017. The Oceanic Nio Index (ONI, Golden Gate Weather Services) indicates that the 11-year period, or the 10-year period from 2006 to 2016, includes one strong (2009–2010) and one very strong (2015–2016) El Niño events and two strong (2007–2008, 2010–2011) and one moderate (2011–2012) La Niña events. El Niño years correspond to the highest tropical mean surface temperature and La Niña years to the lowest.

3. Evidence for PHAT and the Stability Iris Effect

We consider yearly means, computed by averaging each year from July to June, in order to capture the response to El Niño-/La Niña-induced surface temperature changes, that will be maximum during boreal winter (we compute tropically averaged yearly anomalies as $\langle x\rangle_{year} - \langle x\rangle_{2006-2016}$, where the overbar denotes tropical averaging, brackets denote time averaging, *year* refers to each year within 2006–2016, and x can be Z_{anv}, T_S, Z_{D_r}, or other variables).

On the tropical and interannual scales, strong correlations of Z_{anv} and Z_{D_r} with the tropical mean surface temperature confirm that both anvils and D_r rise as the tropics warm ($r = 0.87$ and $r = 0.94$, respectively, Figures 2a and 2b). The altitudes of both anvils and D_r are the highest during the very strong 2015–2016 El Niño, relative to the rest of the 10-year record, with anvils forming about 100 m higher than on average (Figure 2a). During that very strong El Niño year, the air temperature at around 12 km increased by about 0.84 K relative to the 10-year average, while the anvil temperature remained at approximately the same temperature, changing by less than 0.01 K (not shown). The altitude of anvils varies in phase with the altitude of the divergence peak D_r, as shown by the correlation of $r = 0.95$ between Z_{anv} and Z_{D_r}, with a slope that is not

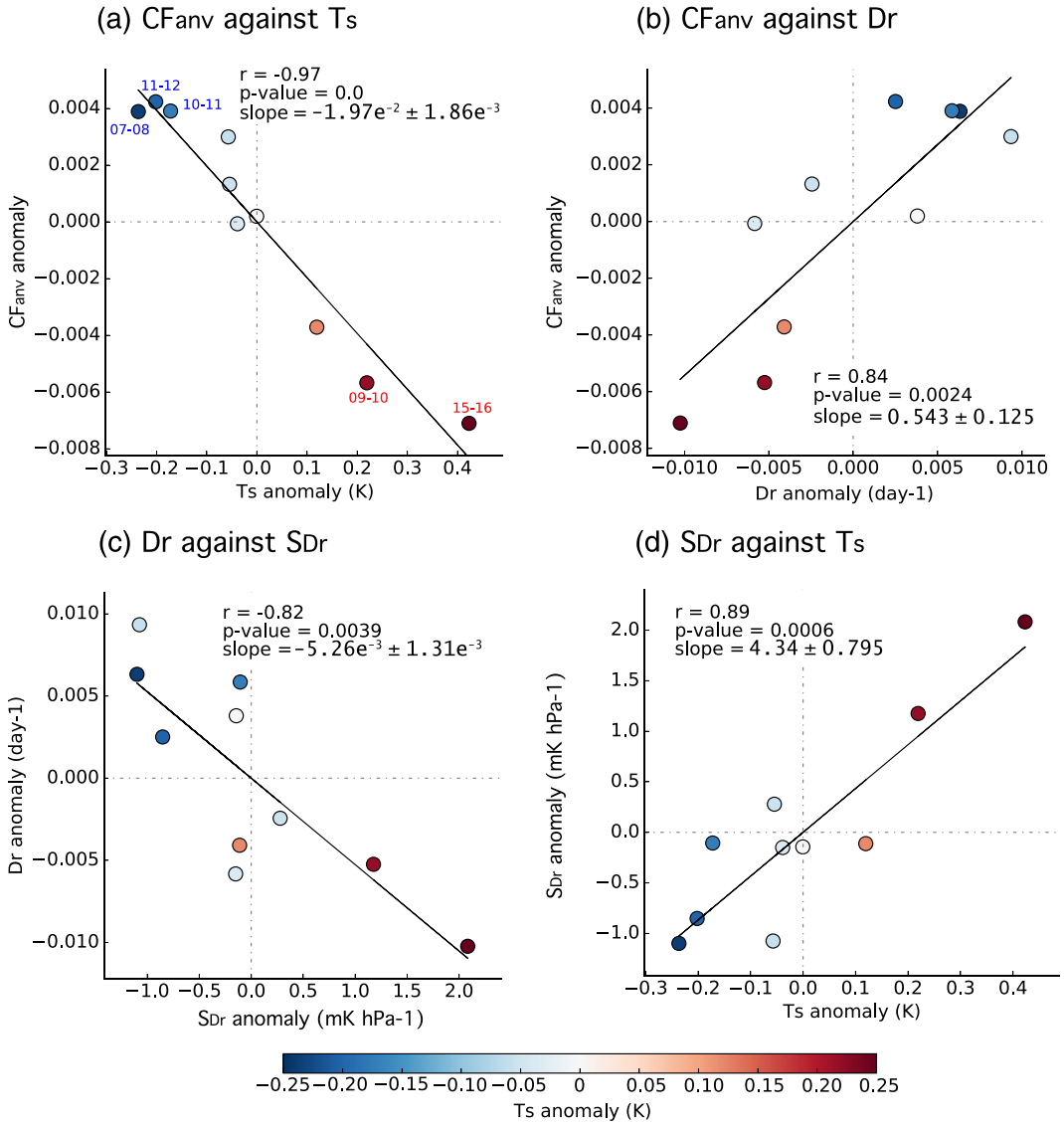

Figure 3. As Figure 2, but for other relationships involving the anvil cloud fraction CF_{anv}, the divergence peak D_r, the tropical mean surface temperature T_S, and the stability at D_r level (S_{D_r}).

statistically different from 1 (Figure 2c). All these findings support the PHAT hypothesis. Note that models rather predict that anvils migrate more than the divergence peak (Zelinka & Hartmann, 2010).

In addition to PHAT, Figure 3a shows that tropical warming is associated with a reduced anvil coverage (negative correlation between CF_{anv} and T_s, $r = -0.97$). This supports the existence of an Iris effect, as defined by a reduction of anvil coverage associated with tropical warming.

Moreover, the decrease of anvil coverage is associated with a weakening of the radiative divergence peak D_r, as shown by the correlation between CF_{anv} and D_r of $r = 0.84$ (Figure 3b). This supports the idea that anvils are tightly linked to the peak of the radiatively driven clear-sky convergence: not only their altitudes but also their amplitudes vary in phase.

As the clear-sky radiative cooling profile (Q_r) shifts upward, the vertical gradient of the radiatively driven subsidence ($\partial\omega_r/\partial p$) becomes less steep because of the stronger stability (S), which weakens the divergence peak D_r (Equation 1). This is supported by the negative correlation between D_r and the stability at the level of D_r (S_{D_r}), of $r = -0.82$ (Figure 3c). This all happens in response to tropical warming, as shown by the

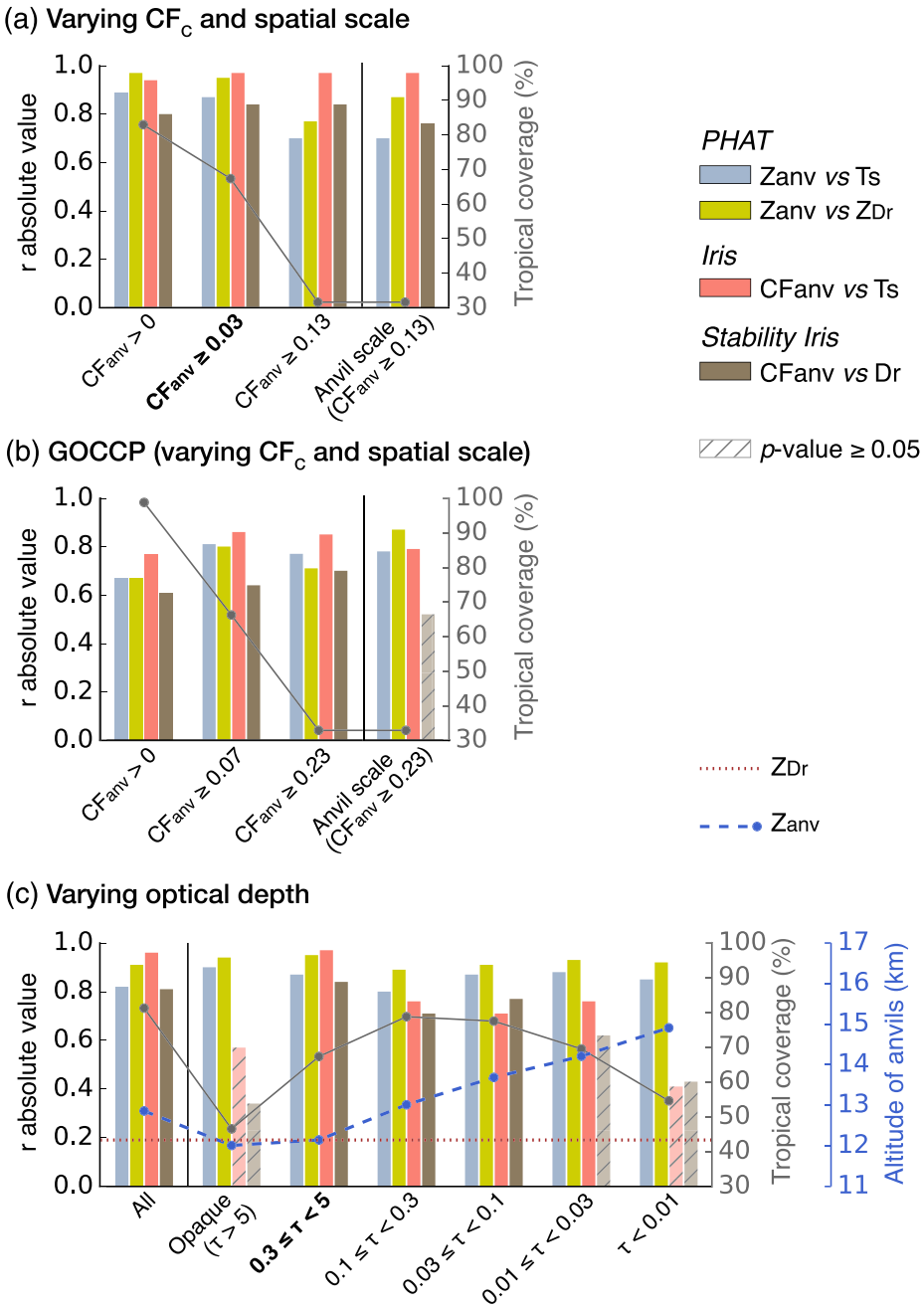

Figure 4. Evolution of linear regressions shown on Figures 2a, 2c, 3a, and 3b with varying critical cloud fraction CF_c and spatial scale, with CALIPSO-Cloud-Occurrence (a) and GOCCP (b), and with varying optical depths of selected anvils (c). Color bars give the absolute value of the Pearson correlation coefficients r. Hatched light bars indicate p value ≥ 0.05. The grey line gives the average percentage of the tropics covered by identified anvils. (a, b) The last case (anvil scale) is when the definition of T_S, D_r, and Z_{D_r} is restricted to locations with anvils. (c) Only clouds of a certain range of optical depths (τ) are considered, above 8 km: all clouds (ice and water), ice opaque clouds, and ice non-opaque clouds within different τ ranges. The dashed blue line gives the average altitude of selected anvils Z_{anv} in annual mean. The dotted brown horizontal line indicates the annual mean value of Z_{D_r}, averaged over the whole tropics. (a, c) Categories in bold correspond to the results shown in section 3.

correlation between S_{D_r} and T_s of $r = 0.89$ (Figure 3d). To summarize, the reduction of both D_r and CF_{anv} is associated with an increase of static stability at the height of anvils, in response to tropical warming. Although causality cannot be determined from observations, these relationships are fully consistent with the stability Iris mechanism.

4. Spatial Scale and Robustness of the Observed Relationships

4.1. Varying Critical Anvil Cloud Fraction, Spatial Scale, and Vertical Resolution

To test the robustness of our results, we assess the sensitivity of the PHAT relationships shown on Figures 2a and 2c (Z_{anv} against T_S and against Z_{D_r}), the Iris effect, and the stability Iris effect relationships shown on Figures 3a and 3b (CF_{anv} against T_S and against D_r), to the value of the CF_c threshold used to identify anvils. Using $CF_c = 0$ (i.e., CF_{anv}%3E0) means that anvils are defined where there is a cloud fraction maximum in the upper troposphere without any constraint on the magnitude of this maximum (in this case, anvils are present in about 83% of the $2° \times 2.5°$ grid points of the tropics on average), while using $CF_c = 0.13$ (i.e., $CF_{anv} \geq 0.13$) means that anvils are only detected where the cloud fraction maximum in the upper troposphere exceeds 0.13 (represents about 30% of the $2° \times 2.5°$ grid points of the tropics on average, Figure 4a). Figure 4a shows that all relationships remain strong ($|r| \geq 0.7$) and significant (p value %3C 0.05) for CF_c ranging from 0 to 0.13, meaning that our results are independent of the value used for CF_c.

PHAT and the stability Iris hypothesis relate the altitude and coverage of anvils to the radiatively driven convergence in surrounding clear-sky regions. However, the scale of this "surrounding" is unclear. The clear-sky regions (hence D_r and Z_{D_r}) are so far considered over the whole tropical belt in all cases (30°N–30°S). The PHAT, Iris, and stability Iris relationships are thus already shown to be well observed at the tropics scale, since they remain strong even when some clear-sky regions are remote from the identified anvils (for all values of CF_c). Thompson et al. (2017) observed that PHAT holds on zonal averages at each latitude. This leads to the following question: over which spatial scale does the balance between clear-sky convergence and convective detrainment hold?

To answer this question, we now restrict the clear-sky regions to the immediate vicinity of anvils. For this purpose, D_r and Z_{D_r} are computed only on locations where anvils have been detected with CF_c=0.13, the highest of the values considered here (surface temperature is averaged over the same locations). Using CF_c=0.13 excludes remote regions with small or no anvils such as the subtropics: clear-sky radiative quantities are then only considered within the same grid points as anvils with a strong cloud fraction, making it possible to investigate the relationships at the anvil (or local) scale. The corresponding correlation coefficients are shown on Figure 4a at the extreme right of the plot and remain strong and significant for all four relationships. The same results are obtained when using the total cloud fraction (i.e., not restricting to ice thick non-opaque clouds), with all correlations remaining strong and significant for the whole range of spatial scales (not shown). The PHAT, Iris, and stability Iris relationships thus hold both at the large scale, such as those of the Hadley-Walker circulations, and at the scale of the close surroundings of the anvils, within a few hundred kilometers.

We now replicate this analysis with the GCM-oriented GOCCP product, which detects and diagnoses the total cloud fraction assuming a coarser vertical resolution of the lidar backscatter signal, of 480 m instead of 60 m. Here again, depending on the CF_c threshold used to define anvils, anvils cover either 99% ($CF_c = 0$), or about 70% ($CF_c = 0.07$), or about 30% ($CF_c = 0.23$) of the $2° \times 2°$ grid points of the tropics on average (Figure 4b). Although all four correlations weaken with GOCCP, they are still significant when anvils cover 99%, 70%, or 30% of the tropics ($|r|$%3E0.6). Only at the anvil scale, where clear-sky regions are restricted to the immediate vicinity of anvils selected with a strong threshold ($CF_c = 0.23$), evidence of the stability Iris effect becomes faint but is still detectable ($r = 0.52$ with p value = 0.0992). Therefore, the PHAT, Iris, and stability Iris relationships remain detectable with a degraded vertical resolution of about 500 m, although with better significance when clear-sky regions encompass more than the immediate vicinity of anvils.

4.2. Influence of the Anvil Optical Depth

So far, our definition of anvil clouds has been restricted to thick but non-opaque ice clouds ($0.3 \leq \tau$%3C5). Figure 4c compares the correlation coefficients for the PHAT, Iris, and stability Iris relationships when using a range of optical depths. Note that the value of CF_c is adapted in each case to remain proportional to the maximum of the annual mean tropically averaged cloud fraction profile; practically, $CF_c = 0.42 \times \max(\langle \overline{CF} \rangle)$. As the optical depth decreases, the altitude of the selected clouds increases, going up to 15 km for thin ice clouds (τ%3C0.01), consistent with the persistent occurrence of subvisible cirrus clouds near the tropical tropopause (e.g., Jensen et al., 1996, 1999; Wang et al., 1994). On the other hand, the altitude of opaque ice clouds, which correspond to the cores of deep convective clouds, is around 12 km.

The PHAT relationships remain strong and significant for all optical depths (r%3E0.7), meaning that the altitude of all high clouds (opaque, thick, or thin) is correlated with T_S and Z_{D_r}. PHAT thus seems to hold for anvils as well as for high cirrus clouds, which is consistent with the vertical structure of the atmosphere, including cirrus clouds near the tropopause, rising approximately in step with the atmospheric isotherms as the tropics warm (Gage & Reid, 1986; Lu et al., 2008).

The Iris and stability Iris relationships remain strong and significant for most non-opaque ice clouds ($|r|$%3E0.7 for $\tau \geq 0.03$), except for high subvisible cirrus clouds ($|r|$%3C0.5 for τ%3C0.01). This is consistent with the fact that the formation of subvisible cirrus clouds is associated with mechanisms different from deep convection (Fueglistaler et al., 2009). The Iris and stability Iris relationships are also weak and non-significant for ice opaque clouds (0.5%3C$|r|$%3C0.6 for Iris and r%3C0.4 for stability Iris), which are found at the deepest cores of convective systems. This suggests that the cloud fraction of deep convective cores is less constrained by the upper tropospheric clear-sky mass divergence than the cloud fraction of detrained anvils.

5. Conclusions

Interannual variations of the anvils cloud fraction, inferred from 10 years of CALIPSO measurements, show that the anvil coverage is reduced when the tropics are anomalously warm. ERA5 reanalyses further show that the altitude and extent of anvils vary in phase with the altitude and strength of the radiatively driven clear-sky mass convergence peak and that both are tightly linked to the static stability profile. As the tropics warm, the peak of the clear-sky radiatively driven mass convergence rises and weakens because of the increase in stability with height, resulting in a reduced anvil cloud fraction. High subvisible cirrus clouds and deep convective clouds also rise in step with temperature, but only the cloud fraction of anvil clouds is reduced with warming, consistent with the stability Iris effect. Robust, consistent, and highly significant relationships derived from 10 years of CALIPSO observations provide a strong observational support for both the PHAT and the stability Iris hypotheses. Observations further show that PHAT and the stability Iris effect hold over a large range of spatial scales. This suggests that clear-sky regions can influence anvils both in the vicinity of clouds and remotely over long distances.

At the interannual scale, tropical warming anomalies generally coincide with El Niño events. Although the interannual and the longer-term climate change responses to tropical warming cannot be directly compared, theoretically, PHAT and the stability Iris effect can hold in both contexts. Whether or not the relationship with temperature shown here actually applies to longer-term global warming remains an open question. Beyond surface warming, anthropogenically induced changes in upper tropospheric CO_2 and ozone concentrations might change the static stability profile and thus potentially overwhelm the stability Iris effect (Harrop & Hartmann, 2012). CO_2-induced changes in the atmospheric overturning circulation (Bony et al., 2013) could also influence the altitude and coverage of tropical anvils. The continuation of space-borne lidar measurements on the long term will allow us to monitor these changes. Although the evidence for the stability Iris effect is stronger when using highly vertically resolved lidar measurements, it remains when using data at coarser vertical resolutions. This suggests that GOCCP could be used to test the ability of climate models to reproduce this effect. This will constitute a necessary, albeit not sufficient, test of the credibility of the predicted behavior of anvil clouds with temperature in the models.

Finally, we emphasize that the stability Iris hypothesis does not imply anything about the radiative impact of the anvil behavior. The rise of anvils with warming is known to produce a positive climate feedback (Zelinka & Hartmann, 2010). The decrease of anvil coverage with warming can be associated with both an increase in the outgoing long-wave radiation and a decrease in planetary albedo. It can also enhance the exposure to space of low-level clouds, which may also impact the overall planetary albedo. Whether one effect dominates over the other is unknown a priori and will require a specific study.

Data Availability Statement

ERA5 (Fifth generation of ECMWF atmospheric reanalyses of the global climate) is available at https://cds.climate.copernicus.eu/cdsapp#!/home. CALIPSO level 3 cloud occurrence is available at https://eosweb.larc.nasa.gov/project/calipso/cal_lid_l3_cloud_occurrence_v1-00. GOCCP is available at https://climserv.

ipsl.polytechnique.fr/cfmip-obs/Calipso_goccp.html. The Met Office HadCRUT4 product is available at https://www.metoffice.gov.uk/hadobs/hadcrut4/.

Acknowledgments
We thank the two anonymous reviewers for their suggestions, which helped to substantially improve the manuscript. MSL is funded by CNES. SB and JLD are supported by the European Unions Horizon 2020 research and innovation program under grant agreements 694768 (ERC project EUREC4A) and 820829 (CONSTRAIN project). This work was supported by CNES. It is based on observations with CALIOP embarked on CALIPSO. To process the CALIPSO, GOCCP, and ERA5 data, this study benefited from the IPSL mesocenter ESPRI facility which is supported by CNRS, Sorbonne Université, Labex L-IPSL, CNES, and Ecole Polytechnique.

References

Bony, S., Bellon, G., Klocke, D., Sherwood, S., Fermepin, S., & Denvil, S. (2013). Robust direct effect of carbon dioxide on tropical circulation and regional precipitation. *Nature Geoscience*, *6*(6), 447–451. https://doi.org/10.1038/ngeo1799

Bony, S., Stevens, B., Coppin, D., Becker, T., Reed, K. A., Voigt, A., & Medeiros, B. (2016). Thermodynamic control of anvil cloud amount. *Proceedings of the National Academy of Sciences*, *113*(32), 8927–8932. https://doi.org/10.1073/pnas.1601472113

Bony, S., Stevens, B., Frierson, D. M. W., Jakob, C., Kageyama, M., Pincus, R., et al. (2015). Clouds, circulation and climate sensitivity. *Nature Geoscience*, *8*(4), 261–268. https://doi.org/10.1038/ngeo2398

Chepfer, H., Bony, S., Winker, D., Cesana, G., Dufresne, J. L., Minnis, P., et al. (2010). The GCM-Oriented CALIPSO Cloud Product (CALIPSO-GOCCP). *Journal of Geophysical Research*, *115*, D00H16. https://doi.org/10.1029/2009JD012251

Choi, Y.-S., Kim, W., Yeh, S.-W., Masunaga, H., Kwon, M.-J., Jo, H.-S., & Huang, L. (2017). Revisiting the Iris effect of tropical cirrus clouds with TRMM and A-Train satellite data. *Journal of Geophysical Research: Atmospheres*, *122*, 5917–5931. https://doi.org/10.1002/2016JD025827

Cronin, T. W., & Wing, A. A. (2017). Clouds, circulation, and climate sensitivity in a radiative-convective equilibrium channel model. *Journal of Advances in Modeling Earth Systems*, *9*, 2883–2905. https://doi.org/10.1002/2017MS001111

Del Genio, A. D., & Kovari, W. (2002). Climatic properties of tropical precipitating convection under varying environmental conditions. *Journal of Climate*, *15*(18), 2597–2615. https://doi.org/10.1175/1520-0442(2002)015%3C2597:CPOTPC%3E2.0.CO;2

Eitzen, Z. A., Xu, K.-M., & Wong, T. (2009). Cloud and radiative characteristics of tropical deep convective systems in extended cloud objects from CERES observations. *Journal of Climate*, *22*(22), 5983–6000. https://doi.org/10.1175/2009JCLI3038.1

Fueglistaler, S., Dessler, A. E., Dunkerton, T. J., Folkins, I., Fu, Q., & Mote, P. W. (2009). Tropical tropopause layer. *Reviews of Geophysics*, *47*, RG1004. https://doi.org/10.1029/2008RG000267

Gage, K. S., & Reid, G. C. (1986). The tropical tropopause and the El Niño of 1982–1983. *Journal of Geophysical Research*, *91*(D12), 13,315–13,317. https://doi.org/10.1029/JD091iD12p13315

Harrop, B. E., & Hartmann, D. L. (2012). Testing the role of radiation in determining tropical cloud-top temperature. *Journal of Climate*, *25*(17), 5731–5747. Publisher: American Meteorological Society. https://doi.org/10.1175/JCLI-D-11-00445.1

Hartmann, D. L. (2016). Tropical anvil clouds and climate sensitivity. *Proceedings of the National Academy of Sciences*, *113*(32), 8897–8899. https://doi.org/10.1073/pnas.1610455113

Hartmann, D. L., & Larson, K. (2002). An important constraint on tropical cloud-climate feedback. *Geophysical Research Letters*, *29*(20), 1951. https://doi.org/10.1029/2002GL015835

Hartmann, D. L., & Michelsen, M. L. (2002). No evidence for Iris. *Bulletin of the American Meteorological Society*, *83*(2), 249–254. https://doi.org/10.1175/1520-0477(2002)083%3C0249:NEFI%3E2.3.CO;2

Hersbach, H., Bell, B., Berrisford, P., Horányi, A., Muñoz Sabater, J., Nicolas, J., et al. (2019). Global reanalysis: Goodbye ERA-Interim, hello ERA5, ECMWF Newsletter, No. 159, ECMWF. *ECMWF Newsletter*, *159*, 17–24.

Jensen, E. J., Read, W. G., Mergenthaler, J., Sandor, B. J., Pfister, L., & Tabazadeh, A. (1999). High humidities and subvisible cirrus near the tropical tropopause. *Geophysical Research Letters*, *26*(15), 2347–2350. https://doi.org/10.1029/1999GL900266

Jensen, E. J., Toon, O. B., Selkirk, H. B., Spinhirne, J. D., & Schoeberl, M. R. (1996). On the formation and persistence of subvisible cirrus clouds near the tropical tropopause. *Journal of Geophysical Research*, *101*(D16), 21,361–21,375. https://doi.org/10.1029/95JD03575

Khairoutdinov, M., & Emanuel, K. (2013). Rotating radiative-convective equilibrium simulated by a cloud-resolving model. *Journal of Advances in Modeling Earth Systems*, *5*, 816–825. https://doi.org/10.1002/2013MS000253

Kubar, T. L., Hartmann, D. L., & Wood, R. (2007). Radiative and convective driving of tropical high clouds. *Journal of Climate*, *20*(22), 5510–5526. https://doi.org/10.1175/2007JCLI1628.1

Li, Y., Yang, P., North, G. R., & Dessler, A. (2012). Test of the fixed anvil temperature hypothesis. *Journal of the Atmospheric Sciences*, *69*(7), 2317–2328. https://doi.org/10.1175/JAS-D-11-0158.1

Lindzen, R. S., Chou, M.-D., & Hou, A. Y. (2001). Does the Earth have an adaptive infrared Iris? *Bulletin of the American Meteorological Society*, *82*(3), 417–432. https://doi.org/10.1175/1520-0477(2001)082%3C0417:DTEHAA%3E2.3.CO;2

Liu, R., Liou, K.-N., Su, H., Gu, Y., Zhao, B., Jiang, J. H., & Liu, S. C. (2017). High cloud variations with surface temperature from 2002 to 2015: Contributions to atmospheric radiative cooling rate and precipitation changes. *Journal of Geophysical Research: Atmospheres*, *122*, 5457–5471. https://doi.org/10.1002/2016JD026303

Lu, J., Chen, G., & Frierson, D. M. W. (2008). Response of the zonal mean atmospheric circulation to El Niño versus global warming. *Journal of Climate*, *21*(22), 5835–5851. Publisher: American Meteorological Society. https://doi.org/10.1175/2008JCLI2200.1

Mauritsen, T., & Stevens, B. (2015). Missing Iris effect as a possible cause of muted hydrological change and high climate sensitivity in models. *Nature Geoscience*, *8*(5), 346–351. https://doi.org/10.1038/ngeo2414

Morice, C. P., Kennedy, J. J., Rayner, N. A., & Jones, P. D. (2012). Quantifying uncertainties in global and regional temperature change using an ensemble of observational estimates: The HadCRUT4 data set: THE HADCRUT4 DATASET. *Journal of Geophysical Research*, *117*, D08101. https://doi.org/10.1029/2011JD017187

Stephens, G., Winker, D., Pelon, J., Trepte, C., Vane, D., Yuhas, C., et al. (2017). CloudSat and CALIPSO within the A-Train: Ten years of actively observing the Earth system. *Bulletin of the American Meteorological Society*, *99*(3), 569–581. https://doi.org/10.1175/BAMS-D-16-0324.1

Su, H., Jiang, J. H., Neelin, J. D., Shen, T. J., Zhai, C., Yue, Q., et al. (2017). Tightening of tropical ascent and high clouds key to precipitation change in a warmer climate. *Nature Communications*, *8*, 15771. https://doi.org/10.1038/ncomms15771

Thompson, D. W. J., Bony, S., & Li, Y. (2017). Thermodynamic constraint on the depth of the global tropospheric circulation. *Proceedings of the National Academy of Sciences*, *114*(31), 8181–8186. https://doi.org/10.1073/pnas.1620493114

Tompkins, A. M., & Craig, G. C. (1999). Sensitivity of tropical convection to sea surface temperature in the absence of large-scale flow. *Journal of Climate*, *12*(2), 462–476. https://doi.org/10.1175/1520-0442(1999)012%3C0462:SOTCTS%3E2.0.CO;2

Wang, P.-H., McCormick, M. P., Poole, L. R., Chu, W. P., Yue, G. K., Kent, G. S., & Skeens, K. M. (1994). Tropical high cloud characteristics derived from SAGE II extinction measurements. *Atmospheric Research*, *34*(1), 53–83. https://doi.org/10.1016/0169-8095(94)90081-7

Winker, D. (2018). CALIPSO lidar level 3 cloud occurrence data, Standard V1-00 [Data set]. NASA Langley Atmospheric Science Data Center DAAC. https://doi.org/10.5067/CALIOP/CALIPSO/L3CLOUDOCCURRENCE-STANDARD-V1-00

Winker, D., Chepfer, H., Noel, V., & Cai, X. (2017). Observational constraints on cloud feedbacks: The role of active satellite sensors. *Surveys in Geophysics*, *38*(6), 1483–1508. https://doi.org/10.1007/s10712-017-9452-0

Winker, D., Hunt, W. H., & McGill, M. J. (2007). Initial performance assessment of CALIOP. *Geophysical Research Letters*, *34*, L19803. https://doi.org/10.1029/2007GL030135

Xu, K.-M., Wong, T., Wielicki, B. A., Parker, L., & Eitzen, Z. A. (2005). Statistical analyses of satellite cloud object data from CERES. Part I: Methodology and preliminary results of the 1998 El Niño/2000 La Niña. *Journal of Climate*, *18*(13), 2497–2514. https://doi.org/10.1175/JCLI3418.1

Xu, K.-M., Wong, T., Wielicki, B. A., Parker, L., Lin, B., Eitzen, Z. A., & Branson, M.(2007). Statistical analyses of satellite cloud object data from CERES. Part II: Tropical convective cloud objects during 1998 El Niño and evidence for supporting the fixed anvil temperature hypothesis. *Journal of Climate*, *20*(5), 819–842. https://doi.org/10.1175/JCLI4069.1

Yuan, J., Houze, R. A., & Heymsfield, A. J. (2011). Vertical structures of anvil clouds of tropical mesoscale convective systems observed by CloudSat. *Journal of the Atmospheric Sciences*, *68*(8), 1653–1674. https://doi.org/10.1175/2011JAS3687.1

Zelinka, M. D., & Hartmann, D. L. (2010). Why is longwave cloud feedback positive? *Journal of Geophysical Research*, *115*, D16117. https://doi.org/10.1029/2010JD013817

Zelinka, M. D., & Hartmann, D. L. (2011). The observed sensitivity of high clouds to mean surface temperature anomalies in the tropics. *Journal of Geophysical Research*, *116*, D23103. https://doi.org/10.1029/2011JD016459